Inventory of Supplemental Information

1) **Figure S1** – Expands upon Figure 6, indicating the percent variance explained of each task's FC matrix by resting-state and multi-task FC matrices. This comparison is also performed for each task relative to each other.
2) **Supplemental Experimental Procedures**
3) **Supplemental References**

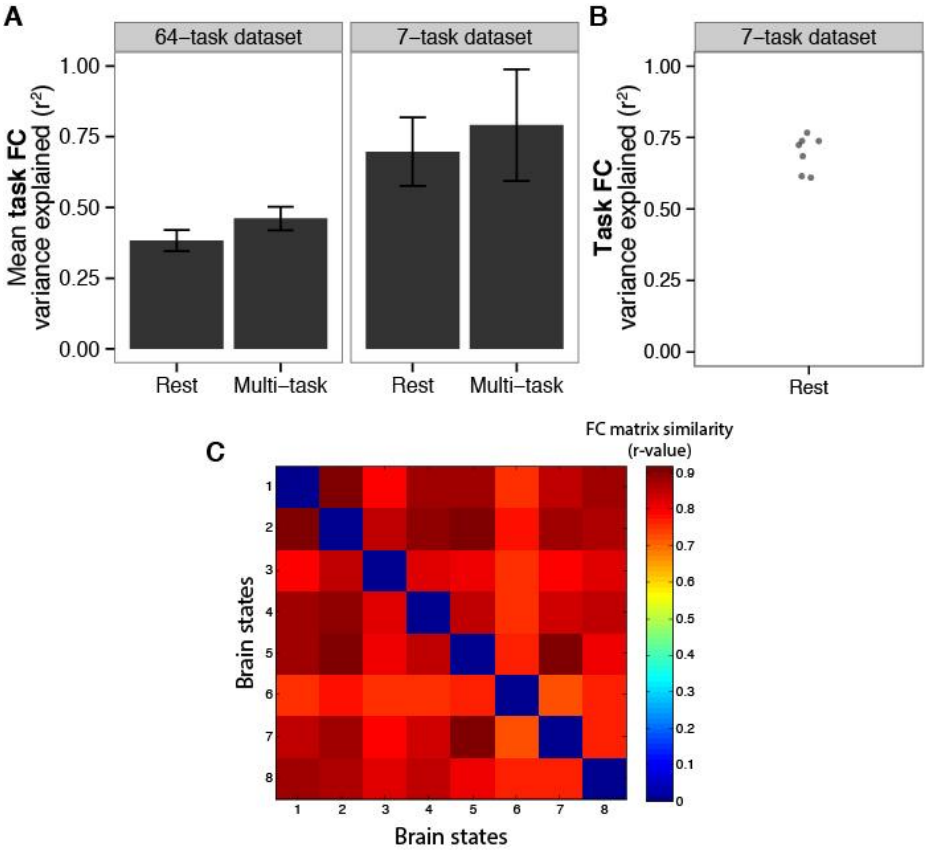

Figure S1 – Amount of task-specific network architecture variance explained by the rest and multi-task network architectures, related to Figure 6. As before, we compared whole-brain FC matrices using Pearson correlations, but we now square the resulting r-values to facilitate inferences regarding percent variance explained. Each task's whole-brain FC matrix was compared to the resting-state FC and multi-task FC matrices (from Figures 3A & 4). **A,** Both resting-state and multi-task FC matrices explained a substantial amount of variance in the FC values across inter-regional connections (the 'network architecture') for each task on average, in both datasets. Error bars indicate inter-task standard deviations. **B**, Each task FC matrix's correlation with the resting-state FC matrix for the 7-task dataset. These are likely the most accurate results given that the most data contributed to both task and rest FC matrices, and given that the resting-state FC matrix does not include potentially arbitrary similarities in FC across tasks (see text for details). Minimum r^2=0.61, maximum r^2=0.77. **C**, Each of the seven task FC matrices are compared to every other (first seven locations, in the order specified in Figure 1B), and to the rest FC matrix (the last location).

SUPPLEMENTAL EXPERIMENTAL PROCEDURES

Task FC estimation. For task data, we sought to suppress or remove influences of (across-trial mean) task-related activations on task-related changes in functional connectivity. Therefore, we ran a standard fMRI general linear model analysis, and calculated FC based on the residuals. Specifically, each region's task time series was modeled using a standard general linear model with one regression coefficient per task. To improve removal of task-related activation variance, a custom hemodynamic response function was used for each subject, based on mean visual region activations to visual events and motor region activations to motor events, as done previously (Aguirre et al., 1998; Cole et al., 2013). For the 7-task dataset, a canonical hemodynamic response function was used, given the inability to estimate hemodynamic shape with a block design. A separate regressor was included for each major 7-task dataset condition (e.g., face stimuli vs. tool stimuli in the N-back task; 24 regressors total). The residuals from this regression model were used for FC estimation, restricted to time points corresponding to the current task (including a standard hemodynamic lag). Note that regressing out task events using general linear modeling primarily removes the across-trial signal means, retaining trial-to-trial and sub-trial fluctuations in time series such that these sources of variability likely contribute the most to task FC estimates (Rissman et al., 2004; Truccolo et al., 2002). Also note that the mean task-related activation confound may have had only a minor effect on results, as removing the activation regression preprocessing step only reduced the 7-task multi-task FC matrix similarity to the resting-state FC matrix (Figure 4) from 0.90 to 0.86.

The residuals from the task activation (GLM) regression model were used for FC estimation, restricted to time points corresponding to the current task (including a standard hemodynamic lag). This step made our approach similar to generalized psycho-physiological interaction (McLaren et al., 2012), except that 1) the task timing regression was run prior to FC calculation rather than simultaneously, 2) an across-condition 'general' regressor was not included (given our interest in intrinsic across-task FC), and 3) FC was measured as Pearson correlations (i.e., covariance normalized by both time series' standard deviations) rather than regression beta coefficients (i.e., covariance normalized by the seed region's variance). We did not use psycho-physiological interaction because of our interest in FC that was consistent across tasks, which is removed in both the standard and generalized psycho-physiological interaction approaches (McLaren et al., 2012; O'reilly et al., 2012).

Estimating percent of FC matrix modification. Each functional connection for each task was compared with that connection during rest (Figure 8A). We applied a Fisher's z-transform to each functional connection and ran a two-tailed t-test (paired by subject), creating a whole-brain FC matrix of p-values for each task. We then corrected this matrix for multiple comparisons using false discovery rate (Genovese et al., 2002) before counting the number of surviving connections and dividing by the total number of connections to get a percentage.

The influence of the amount of data on individual task FC estimates. Unlike the 64-task dataset, for which the intrinsic FC matrices accounted for less than half of the inter-connection variance, in the 7-task dataset over two-thirds of the inter-connection variance was explained (Figure S1). We next assessed whether this was due to the higher amount of data contributing to FC estimates in the 7-task dataset. Consistent with this possibility, the average amount of variance explained by resting-state FC dropped substantially when the same amount of data per subject was used for the 7-task dataset as the 64-task dataset: mean r^2=0.49. When the same number of subjects (N=15) was also used this number dropped further: mean r^2=0.19. This was much more similar to the 64-task dataset result (mean r^2=0.38). These results suggest that the 7-task dataset provides the most accurate estimate of the contribution of intrinsic FC to task FC, as that dataset includes the most data per brain state. We therefore focused primarily on the 7-task dataset for analyses involving individual-task FC estimates.

Static community detection. We used the Louvain locally-greedy algorithm (Blondel et al., 2008; Jutla et al., 2011) for static community detection. We searched over two free parameters to find a community partition for the across-subject mean resting-state FC matrix (**Figure 3A**, right side). The first parameter was the density threshold, whereby weak connections (and all negative connections) were removed prior to running the community detection algorithm. The second parameter was the structural resolution parameter, which can be used to tune the number of communities identified in the FC matrix. The parameter search was conducted across combinations of these two parameters (density of 40% to 2% in increments of 2.5%, and resolution of 1 to 3 in increments of 0.2), with two criteria: 1) there should be a peak of partition similarity (z-score of the Rand coefficient (Traud et al., 2011)) among adjacent locations in this two-dimensional parameter space, and 2) there should be distinct communities corresponding to visual, auditory, default-mode, and motor/tactile systems (given decades of neuroscience research demonstrating their existence). A five-community partition had the highest nearest-neighbor similarity in parameter space, but this did not separate out the auditory system. The next-highest nearest-neighbor similarity peak (density = 9%, resolution = 1.7) was a ten-community partition with distinct communities corresponding to auditory, visual, default-mode, and motor/tactile systems. These parameters were applied to the multi-task average FC matrix, yielding a similar community partition. These partitions were then visualized using Connectome Workbench software (Van Essen et al., 2013) (**Figure 3B**).

Supplemental References

Aguirre, G.K., Zarahn, E., and D'Esposito, M. (1998). The variability of human, BOLD hemodynamic responses. NeuroImage *8*, 360–369.

Blondel, V.D., Guillaume, J.-L., Lambiotte, R., and Lefebvre, E. (2008). Fast unfolding of

communities in large networks. J. Stat. Mech. *2008*, P10008.

Cole, M.W., Reynolds, J.R., Power, J.D., Repovs, G., Anticevic, A., and Braver, T.S. (2013). Multi-task connectivity reveals flexible hubs for adaptive task control. Nat Neurosci *16*, 1348–1355.

Genovese, C., Lazar, N., and Nichols, T. (2002). Thresholding of statistical maps in functional neuroimaging using the false discovery rate. NeuroImage *15*, 870–878.

Jutla, I.S., Jeub, L., and Mucha, P.J. (2011). A generalized Louvain method for community detection implemented in MATLAB. http://netwiki.amath.unc.edu/GenLouvain.

McLaren, D.G., Ries, M.L., Xu, G., and Johnson, S.C. (2012). A generalized form of context-dependent psychophysiological interactions (gPPI): a comparison to standard approaches. NeuroImage *61*, 1277–1286.

O'reilly, J.X., Woolrich, M.W., Behrens, T.E.J., Smith, S.M., and Johansen-Berg, H. (2012). Tools of the trade: psychophysiological interactions and functional connectivity. Social Cognitive and Affective Neuroscience *7*, 604–609.

Rissman, J., Gazzaley, A., and D'Esposito, M. (2004). Measuring functional connectivity during distinct stages of a cognitive task. NeuroImage *23*, 752–763.

Traud, A.L., Kelsic, E.D., Mucha, P.J., and Porter, M.A. (2011). Comparing Community Structure to Characteristics in Online Collegiate Social Networks. SIAM Rev. *53*, 526–543.

Truccolo, W.A., Ding, M., Knuth, K.H., Nakamura, R., and Bressler, S.L. (2002). Trial-to-trial variability of cortical evoked responses: implications for the analysis of functional connectivity. Clin Neurophysiol *113*, 206–226.

Van Essen, D.C., Smith, S.M., Barch, D.M., Behrens, T.E.J., Yacoub, E., Ugurbil, K., and Consortium, F.T.W.-M.H. (2013). The WU-Minn Human Connectome Project: An overview. NeuroImage 1–18.